Electronic structure, magnetism, and antisite disorder in CoFeCrGe and CoMnCrAl quaternary Heusler alloys

Enamullah,[1,*] Y. Venkateswara,[1] Sachin Gupta,[1,2] Manoj Raama Varma,[3] Prashant Singh,[4] K. G. Suresh,[1] and Aftab Alam[1,†]

[1]*Department of Physics, Indian Institute of Technology Bombay, Mumbai 400 076, India*

[2]*Advanced Institute for Materials Research, Tohoku University, Sendai-980-8577, Japan*

[3]*National Institute for Interdisciplinary Sciences and Technology (CSIR), Thiruvananthapuram, India*

[4]*Ames Laboratory, U.S. Department of Energy, Iowa State University, Ames, Iowa 50011-3020, USA*

(Received 7 September 2015; revised manuscript received 15 November 2015; published 10 December 2015)

We present a combined theoretical and experimental study of two quaternary Heusler alloys CoFeCrGe (CFCG) and CoMnCrAl (CMCA), promising candidates for spintronics applications. Magnetization measurement shows the saturation magnetization and transition temperature to be $3\mu_B$, 866 K and $0.9\mu_B$, 358 K for CFCG and CMCA respectively. The magnetization values agree fairly well with our theoretical results and also obey the Slater-Pauling rule, a prerequisite for half metallicity. A striking difference between the two systems is their structure; CFCG crystallizes in fully ordered Y-type structure while CMCA has $L2_1$ disordered structure. The antisite disorder adds a somewhat unique property to the second compound, which arises due to the probabilistic mutual exchange of Al positions with Cr/Mn and such an effect is possibly expected due to comparable electronegativities of Al and Cr/Mn. *Ab initio* simulation predicted a unique transition from half metallic ferromagnet to metallic antiferromagnet beyond a critical excess concentration of Al in the alloy.

DOI: 10.1103/PhysRevB.92.224413 PACS number(s): 75.50.Cc, 61.43.−j, 85.75.−d, 31.15.A−

I. INTRODUCTION

Spintronics technology based on the spin degree of freedom of electrons has potential advantages over conventional electronics, such as high-speed data processing, low power consumption, large circuit integration density, etc., and is rapidly growing [1]. There are many materials such as simple transition-metal oxides (CrO_2, Fe_3O_4), perovskite manganites, transition-metal chalcogenides, diluted magnetic semiconductors, and many Heusler alloys (HAs), which are promising for spintronics applications [1,2]. The striking feature of these materials is their half metallic (HM) property. From the band concept, half metallicity arises due to the existence of finite density of states for one spin subband (majority channel) and a finite band gap for the other (minority channel) at the Fermi level (E_F). The imbalance in the two densities of states results in 100% spin polarization of conduction (majority) electrons at E_F. A ferromagnetic material having HM property is called a HM ferromagnet. Having such type of band structure in the material makes it promising for spin injection and spin manipulation in spintronic devices. Among the systems mentioned, HAs emerge out to be the most favored as HM ferromagnets because of their high Curie temperature (T_C) and structural compatibility [3–6] compared to those of conventional semiconductors. Conventional or full HAs crystallize in the ordered $L2_1$ structure with composition X_2YZ in which X and Y are the transition metals whereas Z is a nonmagnetic element. A new structure arises when one X is replaced by a different transition metal, i.e., the stoichiometry becomes 1 : 1 : 1 : 1 and such alloys are known as quaternary Heusler alloys [7–17] (QHAs) with the formula $XX'YZ$. The resulting compound crystallizes in the LiMgPdSn prototype structure (or Y structure). If Y and Z atoms randomly occupy either of the sites, the resulting structure is $XX'Y_2/XX'Z_2$. Such a structure is referred to as a $L2_1$ disordered structure.

Along with the theoretical prediction of half metallicity in HAs [18], a lot of experimental work on Co-based quaternary HAs have been reported [10,19–21]. In this regard, structural analysis, electronic and magnetic properties, along with the prediction of high spin polarization in QHAs have also been studied experimentally [20]. Element-specific magnetic moments and spin resolved density of states in QHAs are measured using x-ray-absorption spectroscopy [19]. Spin-polarization measurements in CoFeCrAl using point-contact Andreev reflection (PCAR) technique reveals 63% of spin polarized electrons at E_F [21]. It has frequently been observed that among all the Heusler alloys, Co-based HAs are the perfect materials for spintronic applications because of the high value of T_C and spin polarization.

In this paper, we report a detailed theoretical and experimental study of two alloys: CoFeCrGe (CFCG) and CoMnCrAl (CMCA). CFCG is found to have the LiMgPdSn prototype (Y structure) with space group $F\bar{4}3m$ whereas CMCA has $L2_1$ disordered structure. Magnetization measurement shows the saturation magnetization of $3\mu_B$ and $0.9\mu_B$ for CFCG and CMCA respectively, which obeys the Slater-Pauling rule [22,23]. First-principle calculation also yields the same results. In addition, we have also studied the possible effect of antisite disorder ($L2_1$ disorder) between ($Mn_{1-x}Al_{1+x}$) and ($Cr_{1-x}Al_{1+x}$) pairs in CMCA alloy. Interestingly, a unique transition from half metallic to metallic state occurs if we go beyond 3.70% Al excess in both Mn-Al and Cr-Al pairs.

II. EXPERIMENTAL TECHNIQUES AND COMPUTATIONAL DETAILS

A. Experimental techniques

Both the polycrystalline alloys, i.e., CFCG and CMCA were synthesized by arc melting the stoichiometric amounts

*enamullah@phy.iitb.ac.in
†aftab@phy.iitb.ac.in

of constituent elements with purity of at least 99.99% in water cooled copper hearth under high purity argon atmosphere. To compensate the weight loss in CMCA due to Mn evaporation, 2% extra Mn was taken. The formed ingots were melted several times for better mixing. As-cast samples were sealed in evacuated quartz tubes and annealed for 7 days at 800° C followed by ice/water mixture quenching. To check phase purity of samples, x-ray diffraction (XRD) patterns were taken at room temperature, using X'Pert Pro diffractometer with Cu K-α radiation.

XRD analysis is done with the help of FullProf suite that uses the least-square refinement between experimental and calculated intensities. It contains a number of programs such as DICVOl06 for indexing XRD pattern, GFourier for calculating and visualizing electron density within the unit cell, etc., for different purposes in XRD and neutron-diffraction (ND) data analysis. Profile matching well known as Lebail fitting is done by refining the lattice constant, peak profile shape parameters of the pseudo-Voigt function as described in the FullProf manual [24]. GFourier program is used for the calculation and visualization of electron density within the unit cell. The visualization is very useful in identifying the atomic positions of constituent elements within the unit cell for known or unknown crystals, i.e., denser electron density contours indicate the position of a heavier element among the constituent elements in the unit cell. The function to be minimized in the Rietveld method is

$$\chi^2 = \sum_{i=1}^{n} w_i \{y_i - y_{ci}\}^2 \quad (1)$$

with $w_i = 1/\sigma_i^2$, where σ_i^2 is the variance of the " observation" y_i. Here y_i and y_{ci} are the observed and the calculated scattering intensities for a diffraction angle $2\theta_i$ [24]. The smaller the value of χ^2, the better is the refinement.

The patterns for CMCA were the same before and after annealing, but for CFCG alloy, a small amount of secondary phase was seen after annealing. Therefore, as-prepared CFCG and annealed CMCA were used for magnetization $M(H,T)$ measurements. $M(H,T)$ was measured using a physical property measurement system (PPMS) (Quantum Design). High-temperature magnetization measurements were performed with an oven attached to the PPMS.

As discussed in the Introduction, the full Heusler alloy (FHA) structure is comprised of four interpenetrating face-centered-cubic (fcc) sublattices and can be thought of as the superposition of rocksalt (NaCl) and zinc-blende (ZnS) -type structures [25]. In the NaCl structure, each Na(Cl) atom is surrounded by six Cl(Na) atoms whereas in the ZnS structure, each Zn is surrounded by four S atoms and vice versa. The atomic sites of the NaCl structure are called octahedral sites whereas the sites in ZnS are known as tetrahedral sites. The ionic nature of bonds in NaCl arises due to the large difference in the electronegativity values between the constituent elements. The covalent bonding nature arises when the difference in electronegativity values of the constituent elements is very small, e.g., in the ZnS structure. In HAs if one considers most electronegative elements (usually from p block) at a (0,0,0) fcc site, the (1/2,1/2,1/2) fcc site will be occupied by the least electronegative element (usually low valance transition metals) [25]. The remaining two fcc sublattices, i.e., (1/4,1/4,1/4) fcc and (3/4,3/4,3/4) fcc sites, will be occupied by the intermediate electronegative elements among the constituent elements. The same nomenclature for atomic sites is used here also, even though they are not surrounded by the number of atoms that gave the name. For example, octahedral sites (0,0,0) fcc and (1/2,1/2,1/2) fcc are surrounded by eight atoms instead of the six atoms suggested by its name. For a FHA of the type X_2YZ, X atoms are of the intermediate electronegativity values and occupy 8c(1/4,1/4,1/4), [two fcc sublattices with atoms at (1/4,1/4,1/4) and (3/4,3/4,3/4)], the Y occupies 4a(0,0,0) [one fcc sublattice at (0,0,0)], and the Z atom occupies 4b(1/2,1/2,1/2) [one fcc sublattice at (1/2,1/2,1/2)] Wyckoff positions of the space group $Fm\bar{3}m$ [25]. The unit cell can be shifted translationally or rotationally by any amount in the crystal and its structure remains the same. If the unit cell of the above atomic positions is shifted by (1/2,1/2,1/2), new atomic positions will be X at 8c, Y at 4b, and Z at 4a Wyckoff sites. There can be other similar combinations. For the case of QHA, if a Z atom is considered at the 4a(0,0,0) position, the remaining three atoms X, X', and Y will be placed in three different fcc sublattices 4b(1/2,1/2,1/2), 4c(1/4,1/4,1/4), and 4d(3/4,3/4,3/4) in three nondegenerate ways such that there are only three independent atomic arrangements in the Y structure. As discussed, any translation of the unit cell does not change the crystal structure, and shifting of these configurations by (1/4,1/4,1/4), (1/2,1/2,1/2), or (3/4,3/4,3/4) of a unit cell will simply change the origin of the atoms but not the configuration. Three configurations are shown for CFCG in Fig. 1. For example, if the atomic positions of Cr and Co are interchanged in Fig. 1(a), the resulting structure is the same as the initial one because if that primitive cell is inverted along the body diagonal, the atomic arrangements will be the same as the initial one. These are energetically nondegenerate configurations. Similarly the other two configurations in Fig. 1 can be

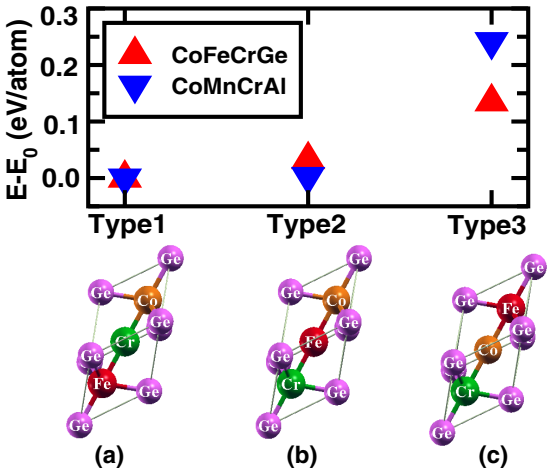

FIG. 1. (Color online) Site preference energy plot for the different configurations of CFCG (triangle up) and CMCA (triangle down). E_0, reference energy, corresponds to type-1 structure. Primitive unit cells (a)–(c) are three nondegenerate configurations of CFCG corresponding to types 1–3.

understood. In this way there are only three nondegenerate (distinct) atomic arrangements for the $XX'YZ$-type quaternary Heusler alloy. The structure factor for the quaternary Heusler alloy $XX'YZ$, having Z at $4a(0,0,0)$, Y at $4b(1/2,1/2,1/2)$, X at $4c(1/4,1/4,1/4)$, and X' at $4d(3/4,3/4,3/4)$ is given below:

$$F_{hkl} = 4(f_z + f_y e^{\pi i(h+k+l)} + f_x e^{\pi/2i(h+k+l)} + f_{x'} e^{-\pi/2i(h+k+l)}) \quad (2)$$

with unmixed (hkl) values. Here f_x, $f_{x'}$, f_y, and f_z are the atomic scattering factors for the atoms X, X', Y, and Z respectively. Therefore,

$$F_{111} = 4[(f_z - f_y) - i(f_x - f_{x'})], \quad (3)$$

$$F_{200} = 4[(f_z + f_y) - (f_x + f_{x'})], \quad (4)$$

$$F_{220} = 4[(f_z + f_y) + (f_x + f_{x'})] \quad (5)$$

are used to classify the ordering of the crystal structure.

B. Computational details

First-principle calculations were done using a spin polarized density functional theory (DFT) implemented within Vienna *ab initio* simulation package (VASP)[26] with a projected augmented-wave basis [27]. We used Perdew-Bueke-Ernzerhof (PBE) for the electronic exchange-correlation functional. 24^3 k mesh was used for Brillouin-zone integration, with a plane-wave cutoff of 288 eV with the energy convergence criteria of 0.1 meV/cell. In order to study the effect of antisite disorder in CMCA, we used a $3 \times 3 \times 3$ supercell involving 108 atoms/cell with 27 atoms of each kind. Guided by the experimental findings, two types of antisite disorder were investigated, i.e., between Mn and Al ($CoMn_{1-x}CrAl_{1+x}$) and Cr and Al ($CoMnCr_{1-x}Al_{1+x}$). Stability of such antisite disorder was checked by calculating the formation energy (ΔE) as defined below for a general $ABCD$ alloy,

$$\Delta E = E[A_{1-x}B_{1+x}CD] - [2(1-x)\,E(A_2CD) + 2(1+x)\,E(B_2CD)]. \quad (6)$$

III. RESULTS AND DISCUSSION

A. Experiment

Rietveld refinement of powder x-ray-diffraction (XRD) data using the FullProf suite reveals that both CFCG and CMCA crystallize in the cubic structure with lattice constants 5.77 ± 0.01 Å and 5.76 ± 0.01 Å, respectively. χ^2 values of Rietveld refinement for three distinct atomic arrangements (as depicted in Fig. 1) are presented in Table I for both the alloys.

TABLE I. χ^2 values of the Rietveld method for three distinct atomic arrangements (from Fig. 1) for CFCG and CMCA.

Alloy/configuration	Type 1	Type 2	Type 3
CFCG	$\chi^2 = 2.04$	$\chi^2 = 2.22$	$\chi^2 = 2.29$
CMCA	$\chi^2 = 1.72$	$\chi^2 = 1.72$	$\chi^2 = 1.99$

For CFCG, the constituent elements are nearest neighbors in the Periodic Table, due to which their atomic scattering factors are nearly identical. Hence the intensities of superlattice peaks (111) and (200) are very small in comparison to that of the (220) peak. This can be understood from Eq. (1). Therefore, one can do the refinement with all the configurations shown in Fig. 1 and can be fitted to XRD data. The best fit between observed and calculated intensities is observed for the first configuration. In this configuration, constituent elements Ge and Cr are at $4a(0,0,0)$ and $4b(1/2,1/2,1/2)$ octahedral sites whereas Co and Fe are at $4c(1/4,1/4,1/4)$ and $4d(3/4,3/4,3/4)$ tetrahedral sites respectively [25]. For CFCG, Cr is the least electronegative (1.66 Pauli units) [28] and therefore it forms an ionic-type sublattice with Ge (which has more electronegativity of 2.01 Pauli units) and becomes stable by donating its electrons to other elements in the alloy. Ge tries to accept electrons from other elements. As a result, the electronic density at the Cr site decreases whereas it increases at the Ge site. The X and X' atoms (here Fe and Co) have intermediate electronegativities and occupy tetrahedral sites [25]. The electronic densities of various atoms in the unit cell can be visualized from the contour plot shown in Fig. 2 generated from XRD refinement. It is clear from Figs. 2(a) and 2(c) that most of the charge is distributed around the Ge atomic site, while the Cr site has the least density. Fe and Co are surrounded by intermediate charge in comparison to Cr and Ge sites in Figs. 2(b) and 2(d). This configuration is energetically most favorable as found from our calculation. Therefore the crystal structure shown in Fig. 1(a) is the most stable.

For CMCA, the superlattice peak (200) is more intense in comparison to the (111) peak and is clearly visible in the XRD pattern (Fig. 3). This suggests that there is a considerable amount of disorder between octahedral sites. This is like the $B2$ disorder in X_2YZ HAs, but in QHAs it should not

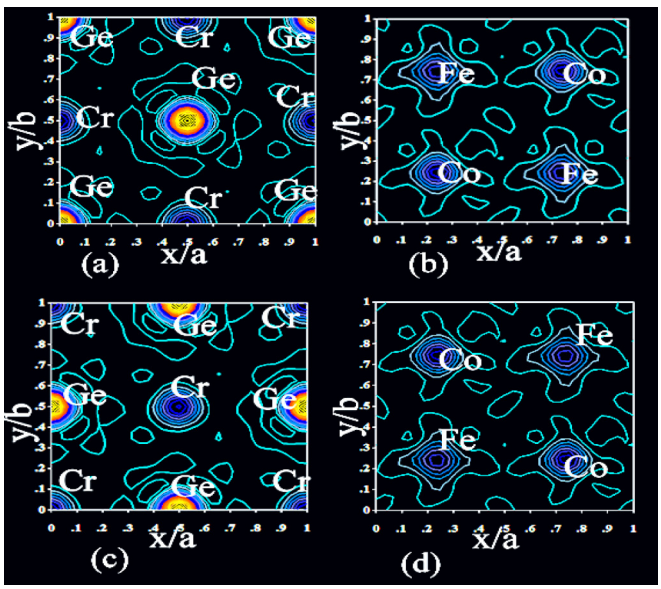

FIG. 2. (Color online) Electronic density of individual atoms in the unit cell of CFCG at (a) $z = 0.0/c$, (b) $z = 0.25/c$, (c) $z = 0.5/c$, and (d) $z = 0.75/c$ plane.

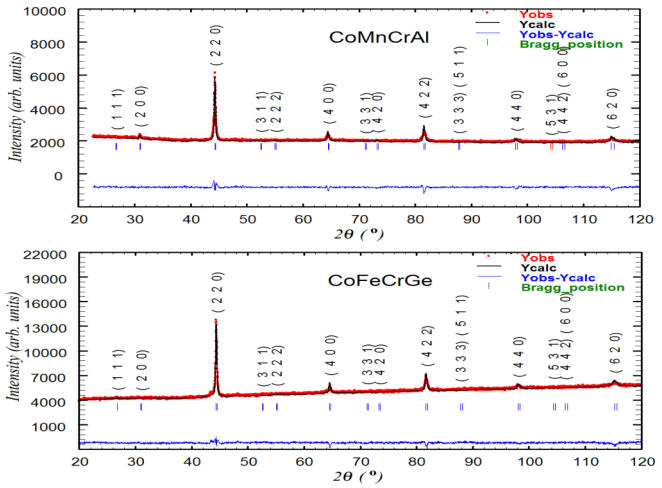

FIG. 3. (Color online) Rietveld refinement of XRD data of CMCA (top) and CFCG (bottom).

be treated as a $B2$ disorder because X and X' are different atoms. It is rather an $L2_1$-type disorder where (0,0,0) and (1/2,1/2,1/2) fcc sublattices are randomly occupied by the Z and Y atoms. From Eq. (1), it is clear that $|F_{111}|^2$ reduces as compared to $|F_{200}|^2$ because $f_z = f_y$ due to equal probability of finding the Z and Y atoms at those sites. Hence the intensity, which is proportional to $|F_{111}|^2 \to 0$ when $|f_x - f_{x'}| \to 0$. Here $|f_x - f_{x'}| \approx 0$ as X and X' are nearest neighbors. Similar to CFCG (Fig. 1), CMCA also has three different configurations with the exception that there is a probability of exchange of atoms between the octahedral sites, i.e., (0,0,0) and (1/2,1/2,1/2) fcc sublattices. Even though XRD can be fitted with all three configurations, the configuration in which octahedral site (1/2,1/2,1/2) fcc contains the least electronegative element is energetically favorable. Here Mn and Cr have the least electronegativity and hence the two configurations [Figs. 1(a) and 1(b)] containing Cr or Mn at (1/2,1/2,1/2) fcc sublattice are favorable. Electronegativity of Al is also of the same order as that of Mn or Cr and consequently Al also tries to occupy at (1/2,1/2,1/2) fcc. As such, Al occupies different octahedral sites (0,0,0) fcc and (1/2,1/2,1/2) fcc. As a consequence the atoms which were initially at (1/2,1/2,1/2) fcc sites occupy both octahedral sites randomly like Al. Due to this behavior, the (111) peak vanishes in XRD. Al atoms occupying (1/2,1/2,1/2) fcc try to lose electrons. Figure 3(b) shows the XRD refinement by considering the equal probability of finding Mn or Al atoms in the octahedral site. The conventional unit cell is shifted by (1/4,1/4,1/4) while doing the refinement and so the space group changes to $Fm\bar{3}m$ (#225). In this space group, the occupancies are Co at 4a, Cr at 4b, and Mn/Al at 8c Wyckoff sites. As Mn and Cr are neighboring elements, swapping of these elements will not be distinguishable from XRD. Due to this reason, the χ^2 value is the same for the first and second configurations, as seen in Table I. Therefore, the conclusion is that CFCG is fully ordered while CMCA has $L2_1$ disordered structure.

It is observed in HAs that if more than one atom has nearly the same electronegative values, some degree of disorder can be expected. For example, CoMnCrAl, CoFeCrAl [8], and $Co_2Cr_{1-x}Fe_xAl$ [29] HAs have disorder between Cr and Al sites. Disorder in these systems arises because of the same electronegativity values of Cr and Al atoms. Consequently the Al atom acts as an electron donor and occupies one of the octahedral sites (1/2,1/2,1/2) fcc with almost the same probability of occupancy as that of Cr atoms. Similarly Mn_2CoAl [30] and Co_2MnAl [31] have a disorder between Mn and Al sites. This type of disorder is seen in HAs containing Zn as well. Zn also tries to occupy both octahedral sites (1/2,1/2,1/2) fcc and (0,0,0) fcc sublattice, because Al and Zn atoms have the nature that in some cases they lose electrons and in some other cases they accept electrons because of their low electronegativity and proximity to the p block of the Periodic Table. However, one can also synthesize perfectly ordered systems in HAs containing Al atoms, such as CoFeTiAl [29] (Y structure) and Co_2TiAl [32] ($L2_1$ structure). The scenario is a bit different in this case. Since the Ti atom has the least electronegativity among the constituent atoms, it behaves as a charge donor and tries to occupy the (1/2,1/2,1/2) fcc and does not allow Al to occupy the same site. Hence there will be no disorder in these systems. Therefore, on the basis of data available on a number of alloys, we could propose an empirical relation between relative electronegativity values and the occurrence of disorder.

The top plots of Fig. 4 show the temperature (T) dependence of magnetization in a constant field of 500 Oe for CFCG (left) and CMCA (right) showing the ferroparamagnetic transition. The Curie temperature has been determined by taking the minima of the first-order derivative of magnetization vs temperature (M-T) curve. The estimated T_C values are about 358 and 866 K for CMCA and CFCG respectively. The high

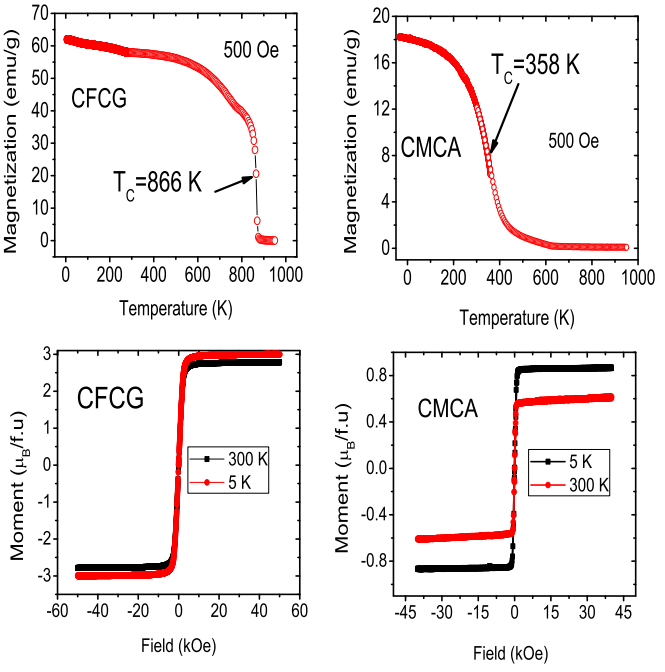

FIG. 4. (Color online) Top: Temperature dependence of magnetization M at 500 Oe. T_C is calculated from the minima of the first-order derivative of M vs T curve. Bottom: Magnetic moment vs H at 300 and 5 K for CFCG (left) and CMCA (right).

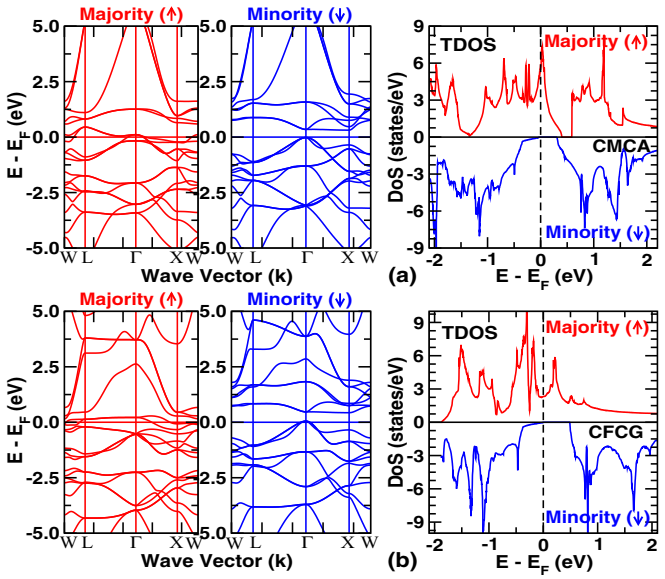

FIG. 5. (Color online) Spin resolved band structure (left) and density of states (right) for CMCA (a) and CFCG (b) at experimental lattice constant (a_{exp}). Both systems clearly show half metallic behavior with a band gap ∼0.328 eV for CMCA and ∼0.481 eV for CFCG.

T_C of these alloys enables them to be potential candidates for room-temperature applications.

Figure 4 (bottom) shows the field dependence of magnetization for the two alloys. The absence of hysteresis reveals the soft magnetic nature of the alloys. Both the alloys show saturation at 5 and 300 K. The saturation moment at 5 K is estimated to be $3\mu_B$ and $0.9\mu_B$ for CFCG and CMCA respectively. The total moment in Heusler compounds can be estimated from the Slater-Pauling rule by counting the number of valence electrons in the primitive cell [33]. In QHA, the total moment (m) per unit cell can be expressed as [10]

$$m = (N_v - 24)\mu_B, \tag{7}$$

where N_v (s,d electrons for transition metals and s,p electrons for main group element) is the number of valence electrons per unit cell. As CFCG and CMCA have 27 and 25 valence electrons respectively, according to the Slater-Pauling rule [using Eq. (7)], the moment in these compounds should be $3\mu_B$ and $1\mu_B$. But the experimentally observed magnetic moment for CMCA ($0.9\mu_B$) slightly deviates from the Slater-Pauling rule, because of the presence of disorder. On the other hand, in CFCG, the agreement is very good. In addition to the experiment, the theoretically calculated moments also agree fairly well with the Slater-Pauling prediction (described in the next section).

B. Theoretical

To check the stability, we have first calculated the site preference energies for various atomic configurations. Considering the symmetry of the $XX'YZ$ structure, we fix the Z atom at the $4d$ position and permute rest of the three atoms on $4a$, $4b$, and $4c$ Wyckoff sites. Out of six possible configurations, only three are energetically nondegenerate, namely types 1–3 as shown in Fig. 1 for both CFCG and CMCA. Type 1 (where the X atom sits at $4a$, X' at $4b$, and Y at $4c$) is found to be energetically the most stable configuration, as also configured by experiment.

Figure 5 shows the spin polarized band structure and density of states (DOS) for CMCA (top) and CFCG (bottom) respectively. Half metallicity is obvious in both systems with a finite state (at E_F) in the majority channel but gapped in minority. The calculated magnetic moment for CMCA is $0.98\mu_B$ ($\mu_{expt} = 0.9\mu_B$) while for CFCG it is $2.99\mu_B$ ($\mu_{expt} = 3.0\mu_B$), which follows the Slater-Pauling rule.

Intrinsic defects such as antisite disorder is fairly common in QHA. Our XRD data clearly indicate the signature of $L2_1$ disorder in CMCA, where the Al site is expected to mix with Mn (and possibly with Cr). The electronic structure of any material is extremely sensitive to such defects, and has not received much attention in the literature. We have performed first-principle calculation to check the stability, electronic structure, and magnetism for two sets of antisite disorders,

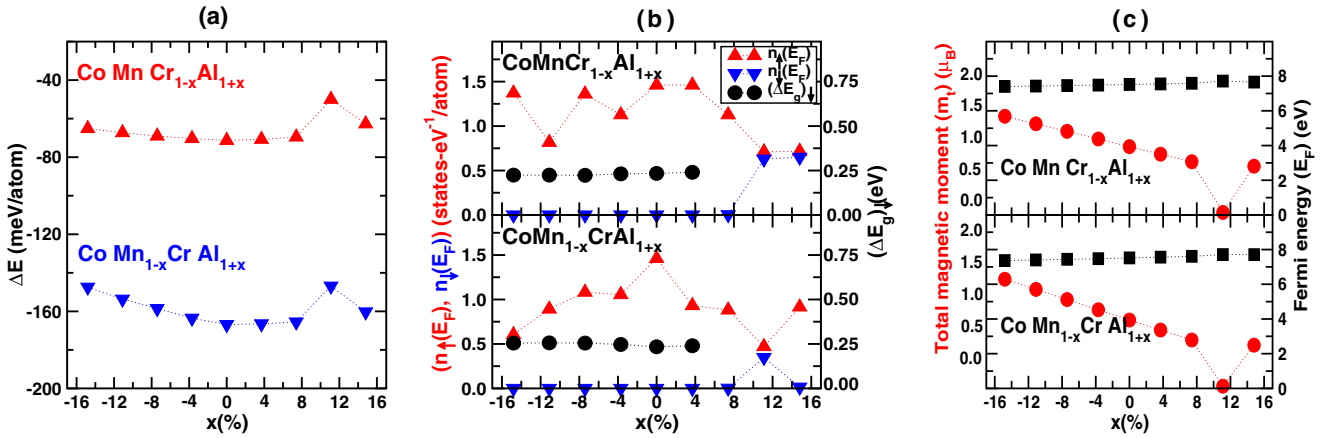

FIG. 6. (Color online) (a) Formation energy (ΔE) vs antisite disorder (x) for $CoMnCr_{1-x}Al_{1+x}$ (up triangle) and $CoMn_{1-x}CrAl_{1+x}$ (down triangle). (b) Concentration (x) dependence of DOS at E_F for majority spin (up triangle), minority spin (down triangle), and band gap $(\Delta E_g)_\downarrow$ (circle) for $CoMnCr_{1-x}Al_{1+x}$ (top) and $CoMn_{1-x}CrAl_{1+x}$ (bottom). (c) x dependence of total magnetic moment (m_t) and change in Fermi energy (E_F) for the same two alloys.

namely $CoMn_{1-x}CrAl_{1+x}$ and $CoMnCr_{1-x}Al_{1+x}$. These are done by using a $3 \times 3 \times 3$ supercell of the primitive four-atom cell.

Figure 6(a) shows the formation energy (ΔE) of $CoMn_{1-x}CrAl_{1+x}$ (down triangle) and $CoMnCr_{1-x}Al_{1+x}$ (up triangle) for both excess (positive x value) and deficit (negative x value) of Al in the compound. Negative values of ΔE indicate that Al indeed prefers to mix with Mn and Cr. Mn is relatively much more preferable to mix due to a larger negative ΔE, as also revealed by our XRD data. Detailed analysis of such antisite disorder can be accurately probed with a neutron-diffraction experiment.

Figure 6(b) shows the value of the DOS at E_F for majority $n_\uparrow$ (up triangle) and minority $n_\downarrow$ (down triangle) spin channels. The associated band gap $(\Delta E_g)_\downarrow$ in the minority spin is also represented (solid circle). The top (bottom) panel is the result for $CoMnCr_{1-x}Al_{1+x}$ ($CoMn_{1-x}CrAl_{1+x}$). Interestingly, a deficit of Al (negative x) up to $x \simeq 14.81\%$ maintains the half metallicity, however an excess of Al (positive x) causes a transition from half metallic to metallic beyond $x \simeq 3.70\%$ in both cases. At 7.41% excess Al, the minority spin tends to have a small DOS at E_F; $n_\downarrow(E_F) \simeq 0.03$ states/eV atom ($CoMnCr_{1-x}Al_{1+x}$) and $n_\uparrow(E_F) \simeq 0.02$ states/eV atom ($CoMn_{1-x}CrAl_{1+x}$).

It turns out that this metallic transition is intimately connected with a magnetic transition, where the system goes from a ferromagnetic state to an antiferromagnetic state. This is shown in Fig. 6(c), where the total magnetic moment changes discontinuously at the same concentration ($x \sim 7.41\%$) at which the system loses its half metallicity. E_F almost remains unchanged with varying x (square symbol). Although we have theoretically studied the effect of antisite disorder up to $x \sim 14.81\%$, such a large disorder may not be expected to survive in the actual sample.

IV. CONCLUSIONS

In conclusion, CFCG and CMCA are found to be two interesting materials; the former crystallizes in a Y-type structure while the latter shows an $L2_1$ disordered structure, which is due to the random occupancy of octahedral site atoms Al with Cr/Mn. Both the alloys show half metallic ferromagnetic behavior with a specific site preference for the constituent atoms. CFCG is more useful because of its high Curie temperature (866 K) while CMCA shows an intrinsic antisite disorder which allows a larger tunability of its properties. Magnetization measurement yields magnetic moments which obey the Slater-Pauling rule, and which also agree with our theoretical prediction in both cases. *Ab initio* electronic structure simulation confirms the stability and half metallicity in both compounds. $L2_1$ disorder in CMCA is further investigated by simulating antisite disorder which also indicates the possibility of half metallic ferromagnetic behavior in the presence of small disorder. However, it changes to a metallic antiferromagnetic state beyond a certain excess Al in the alloy.

ACKNOWLEDGMENTS

Enamullah acknowledges IIT Bombay for providing financial assistance to carry out postdoctoral research. P.S. would like to thank U.S. Department of Energy (DOE), Office of Science, Materials Science and Engineering Division for support.

Enamullah, Y.V., and S.G. contributed equally.

[1] C. Felser, G. H. Fecher, and B. Balke, Angew. Chem., Int. Ed. **46**, 668 (2007).

[2] *Half-Metallic Alloys*, edited by I. Galanakis and P. H. Dederichs (Springer, Berlin, 2005).

[3] R. Farshchi and M. Ramsteiner, J. Appl. Phys. **113**, 191101 (2013).

[4] M. Hashimoto, J. Herfort, H.-P. Schonherr, and K. H. Ploog, Appl. Phys. Lett. **87**, 102506 (2005).

[5] M. Hashimoto, A. Trampert, J. Herfort, and K. H. Ploog, J. Vac. Sci. Technol. B **25**, 1453 (2007).

[6] M. Hashimoto, J. Herfort, A. Trampert, H.-P. Schonherr, and K. H. Ploog, J. Phys. D: Appl. Phys. **40**, 1631 (2007).

[7] L. Bainsla, K. G. Suresh, A. K. Nigam, M. Manivel Raja, B. S. D. Ch. S. Varaprasad, Y. K. Takahashi, and K. Hono, J. Appl. Phys. **116**, 203902 (2014).

[8] L. Bainsla, A. I. Mallick, M. M. Raja, A. K. Nigam, B. S. D. Ch. S. Varaprasad, Y. K. Takahashi, A. Alam, K. G. Suresh, and K. Hono, Phys. Rev. B **91**, 104408 (2015).

[9] K. Ozdogan, E. Sasioglu, and I. Galanakis, J. Appl. Phys. **113**, 193903 (2013).

[10] V. Alijani, J. Winterlik, G. H. Fecher, S. S. Naghavi, and C. Felser, Phys. Rev. B **83**, 184428 (2011).

[11] X. Dai, G. Liu, G. H. Fecher, C. Felser, Y. Li, and H. Liu, J. Appl. Phys. **105**, 07E901 (2009).

[12] M. Singh, H. S. Saini, and M. K. Kashyap, J. Mater. Sci. **48**, 1837 (2013).

[13] V. Alijani, J. Winterlik, G. H. Fecher, S. S. Naghavi, S. Chadov, T. Gruhn, and C. Felser, J. Phys.: Condens. Matter **24**, 046001 (2012).

[14] I. Galanakis, K. Ozdogan, E. Sasioglu, and B. Aktas, Phys. Rev. B **75**, 172405 (2007).

[15] H. Z. Luo, H. W. Zhang, Z. Y. Zhu, L. Ma, S. F. Xu, G. H. Wu, X. X. Zhu, C. B. Jiang, and H. B. Xu, J. Appl. Phys. **103**, 083908 (2008).

[16] I. Galanakis and E. Sasioglu, Appl. Phys. Lett. **99**, 052509 (2011).

[17] M. Meinert, Jan-Michael Schmalhorst, C. Klewe, G. Reiss, E. Arenholz, T. Bohnert, and K. Nielsch, Phys. Rev. B **84**, 132405 (2011).

[18] G. Y. Gao, L. Hu, K. L. Yao, B. Luo, and N. Liu, J. Alloys Compd. **551**, 539 (2013), and references therein.

[19] P. Klaer, B. Balke, V. Alijani, J. Winterlik, G. H. Fecher, C. Felser, and H. J. Elmers, Phys. Rev. B **84**, 144413 (2011).

[20] V. Alijani, S. Ouardi, G. H. Fecher, J. Winterlik, S. S. Naghavi, X. Kozina, G. Stryganyuk, C. Felser, E. Ikenaga, Y. Yamashita, S. Ueda, and K. Kobayashi, Phys. Rev. B **84**, 224416 (2011).

[21] L. Bainsla, A. I. Mallick, A. A. Coelho, A. K. Nigam, B. S. D. Ch. S. Varaprasad, Y. K. Takahashi, A. Alam, K. G. Suresh, and K. Hono, J. Magn. Magn. Mater. **394**, 82 (2015).

[22] J. C. Slater, Phys. Rev. **49**, 931 (1936).
[23] L. Pauling, Phys. Rev. **54**, 899 (1938).
[24] www.ill.eu/sites/fullprof/php/tutorials.html.
[25] T. Graf, C. Felser, and S. S. P. Parkin, Prog. Solid State Chem. **39**, 1 (2011).
[26] G. Kresse and J. Furthmuller, Phys. Rev. B **54**, 11169 (1996); Comput. Mater. Sci. **6**, 15 (1996).
[27] G. Kresse and D. Joubert, Phys. Rev. B **59**, 1758 (1999).
[28] https://en.wikipedia.org/wiki/Electronegativity.
[29] T. Graf and C. Felser, *Spintronics—From Materials to Devices* (Springer, New York, 2013), pp. 33–34.
[30] Y. J. Zhang, G. J. Li, E. K. Liu, and J. L. Chen, J. Appl. Phys. **113**, 123901 (2013).
[31] A. Vinesh, V. D. Sudheesh, N. Lakshmi, and K. Venugopalan, *Solid State Physics: Proceedings of the 58th DAE Solid State Physics Symposium 2013, AIP Conf. Proc. No.* 1591, edited by C. Murli, D. Bhattacharyya, and S. C. Gadkari (AIP, Melville, NY, 2014), p. 1521.
[32] W. Zhang, Z. Qian, Y. Sui, Y. Liu, X. Huang, W. Su, M. Zhang, Z. Liu, G. Liu, and G. Wu, Physica B **367**, 205 (2005).
[33] I. Galanakis, P. H. Dederichs, and N. Papanikolaou, Phys. Rev. B **66**, 174429 (2002).